Light Metals 2011 *Edited by: Stephen J. Lindsay*
TMS (The Minerals, Metals & Materials Society), 2011

Towards Redefining the Alumina Specifications Sheet – The Case of HF Emissions

[1]Linus M. Perander, [2]Marco A. Stam, [1]Margaret M. Hyland, [1]James B. Metson
[1]Light Metals Research Centre, The University of Auckland, New Zealand
[2]Aluminium Delfzijl B.V., Delfzijl, The Netherlands

Alumina quality, HF emissions, Dry-scrubbing, Gibbsite, Residual hydroxide, Pore size distribution

Abstract

For smelting applications, alumina quality is typically defined in terms of chemical and physical properties, with emphasis on impurity elements, surface area, moisture content, particle size distribution and attrition index. However, these properties fail in prediction of the true HF generation potential, as well as the real capacity for HF removal in the dry scrubbers. Using plant measurements and additional laboratory characterization of a number of alumina samples a broadening of how alumina quality is specified is argued for. Measurements of the residual gibbsite/boehmite content and the pore size distribution, coupled with characterization of the alumina microstructure, can be used to predict and understand the generation of HF during feeding and dissolution as well as the ability to capture HF in the dry scrubbers.

Introduction

For both regulatory and process stability reasons, reductions in fluoride emissions from aluminium smelters are an essential part of process improvement. The modern, injection type, dry scrubbing system comprises of a reactor (where alumina is injected and comes in contact with the collected cell off gases) and a separate filtration system (where the reacted alumina and other particulates are separated from the gas stream). These reactors are designed to enable good mixing between gas and solids and can be operated at very high efficiencies with over 99.5 % of the gaseous and particulate fluorides typically being captured [1]. With good pot hood collection efficiency, and the dry scrubber recovering and recycling most of the particulate and gaseous fluorides, the operation may almost be regarded as a closed loop between the cells and the scrubber [2].

The chemistry and mechanism of the dry scrubbing process (i.e. the adsorption and reaction of HF with alumina) was explored in depth by Gillespie [3, 4]. Gillespie argued that since the fluoride adsorption capacity is related to both the specific surface area of the alumina and the relative humidity during the adsorption, the reactions must occur in a surface process. The author presented a mechanism which involved several steps, starting with the adsorption of water on the surface of the alumina followed by HF adsorption and acidification of this surface layer which would dissolve the alumina surface and form AlO_2^- and AlO^{2-} species and finally the precipitation of oxy- and hydroxyfluorides. Most importantly the reaction was shown to be irreversible under dry scrubbing conditions (temperature and atmospheric), an important finding which enabled new developments of the dry scrubbing process and control strategies to be made.

Although the mechanisms for the reaction between HF and alumina (in the dry scrubbing process) are relatively well understood, the role of alumina microstructure and porosity is less clear. There is a direct relationship between the surface area available for adsorption and the adsorption capacity, however it could be expected that the pore size distribution also plays an important role in providing access to internal reaction sites. The porosity and surface area arises from the structure of the transition aluminas which dominate smelter grade aluminas and reflect the incomplete conversion of gibbsite to alpha alumina in the calcination stage [5].

Residual hydroxyls are an integral part of the transition alumina structures (and often reported as LOI). The less calcined the alumina, the higher surface area, and correspondingly, the higher the level of residual hydroxides in the structure. Together with other OH sources (such as gibbsite), these represent the main source of HF formation in the electrolyte [6]. In the cell HF is formed in the electrolytic process when the released water (or OH) reacts with the electrolyte ($NaAlF_3$). It is then easy to see that there is a conflicting relationship between generation of HF from residual hydroxide and capturing the HF by increasing the surface area which inevitably results in more structural hydroxyls and increased HF formation in the first place.

The surface adsorbed water (represented by the MOI values) on the other hand are rapidly flashed off when the alumina is fed into the electrolytic cell [7]. This may actually be beneficial for the dissolution process as it helps with the dispersion of the material [8].

In this paper four alumina samples with very similar specifications, but which demonstrate very different HF emissions levels, are considered. The measurements currently reported on the alumina specification sheet fail to explain this HF generation potential or accurately predict dry-scrubber performance. By using low-cost, and often already existing, laboratory equipment measurements that better account for this may readily be obtained and used to better predict and control the operation, particularly with regards to emissions. This argues for some redefinition of the alumina specifications sheet, particularly when such specifications are used for example in prediction of emissions.

Experimental

The samples examined in this study were obtained during the unloading of the respective alumina shipments and directly from the conveyor belt going to the alumina storage silo. There is only one alumina silo on site which rules out alumina blending as a source of variation. The GTC (Gas Treatment Centre) inlet and outlet HF concentrations are monitored continuously using NEO laser-based gas monitors. This is an infrared single-line absorption spectroscopy measurement which provides a continuous reading of the HF content in the gas stream across the laser path. One laser is mounted in the stack directly after the GTC, and one in each inlet channel to the GTC. The inlet values reported here are averages between these two inlet channels.

TGA experiments were conducted to determine MOI and LOI values, using a Shimadzu TGA-50 apparatus. Approximately 35 mg of each sample was heated, in an open platinum crucible in air, with a constant heating rate of 20 °C min^{-1} from ambient temperature to 1100°C. A baseline curve was also produced, and subtracted from each sample curve, by recording the weight change when an empty platinum crucible was subjected to the same heating conditions as above.

Values for MOI and LOI were obtained based on thermo gravimetric data. As per the ISO standard, the ranges for MOI and LOI were taken as 50-300°C and 300-1000°C, respectively [9]. It should however be pointed out that according to the standard measurement for MOI and LOI values the experiments are performed with a retention time of 2 hours at 300 and 1000°C. The results presented here may therefore not correlate directly to measurements performed according to standard methods but can be used to compare the samples and for calculating the water and hydroxyl content.

Nitrogen porosimetry experiments were conducted to evaluate the specific surface area and pore volume, as well as pore size and pore size distribution. The measurements were performed on a TriStar 3000 apparatus. Approximately 1 gram of sample was used for the analysis. For the measurements the sample is initially degassed under a nitrogen purge at 120°C for 12 hours. Note that in standard analysis different degassing temperatures may be used. The temperature of 120°C was chosen to avoid the reaction of any gibbsite or boehmite present in the sample. The results obtained here thus represent the whole sample as received (without changing its phase composition). The measurements were conducted under liquid nitrogen temperatures and using nitrogen as the adsorbed gas. The BET method [10] was used to evaluate surface area and the BJH method [11] was used for the pore volume and pore size and distribution evaluations.

X-ray diffractometry was performed on a Rigaku apparatus using Cu K-alpha X-rays. The analysis was performed using a 2θ angle of 10-80° and a step width of 0.02°. Rietveld refinement [12, 13] of the diffractograms was then performed using the FullProf software [14]. The fine sub 40 micron size fraction was separated from the bulk by sieving and analysed separately.

X-ray diffractometry with Rietveld refinement allows the alumina phases present in smelter grade aluminas to be quantified. However this technique does not allow the amorphous phases such as rho- or chi-alumina that may affect the performance of the alumina to be measured directly [15, 16]. The highly crystalline phases such as alpha alumina and gibbsite produce sharp, well-defined peaks whereas the less crystalline transition alumina phases produce broader and more diffuse peaks. Several studies report on how the alumina phase composition influences the smelter performance (see for example [17] and references therein).

Results and Discussion

Table 1 displays a selection of properties from the alumina specification sheets for the 4 alumina samples discussed here. It is recognized that other properties are of importance for understanding alumina performance; however, these properties have been chosen as they are most often associated with dry-scrubbing and HF generation, which is the topic of this paper.

Table 1. Alumina properties as reported on the specifications sheet for the 4 alumina samples used in this study.

	Alumina A	Alumina B	Alumina C	Alumina D
LOI (300-1000 °C) wt-%	0.59	0.51	0.79	0.91
BET-SA m2g-1	68.0	66.3	75.6	73.0
Alpha wt-%	N/A	N/A	4.0	5.0
< 20 um wt-%	1.6	1.2	1.9	1.6
Attrition Index	12.0	13.0	4.8	10.87
Bulk Density kgdm-1	1.04	N/A	1.00	0.98

Note that the parameters omitted from the table were not reported on the specifications sheets

Table 1 indicates that aluminas A and B have relatively similar parameters (in terms of MOI, LOI, BET-SA and fines content) which is also to be expected as these samples represent different shipments from the same alumina refinery. Aluminas C and D are different compared to A and B, as they both have higher specific surface areas and LOI values. Alumina C also has a significantly lower attrition index than the rest of the samples.

Based on the parameters reported in table 1 one could expect aluminas A and B to result in similar HF emissions and C and D to perform equally well but perhaps with a higher background HF emission level due to the higher LOI values. Some of the additional HF generated due to the larger amount of structural hydroxyls present in aluminas C and D could be expected to be offset by the significantly higher BET surface areas. However, as Table 2 indicates, these aluminas did not perform as expected. When alumina A was used the fluoride emissions increased by approximately 60 %, compared to alumina B. Similarly, alumina D resulted in twice the emissions compared to alumina C; far more than what could be expected based on the relative LOI values.

Table 2. Associated hydrogen fluoride emissions (total gaseous per hour and fluoride per cubic meter) and scrubber efficiencies.

	Alumina A	Alumina B	Alumina C	Alumina D
Fluoride Emission mg m^{-3}	0.86	0.61	0.56	1.13
Total Gaseous HF Emission kg h^{-1}	1.29	0.92	0.60	1.21
Scrubber Efficiency (%)	N/A	N/A	99.70	99.48

Since HF is generated in an electrochemical reaction between the bath and any hydroxyl species (H_2O, OH^-, NaOH...), a reasonable measure of the HF generation potential is a quantification of the water and hydroxyl content of the aluminas. This is typically done in so called Loss on Ignition and Moisture on Ignition measurements [9], but may also be obtained using thermo-gravimetric analysis techniques. As will be shown the LOI measurement (300-1000°C) does not account for all the OH associated with the alumina.

Figure 1 shows the obtained thermograms for aluminas A and B as well as the thermogram for a standard industrial Bayer gibbsite. It can be seen that the relative weight loss is larger for alumina A, which indicates higher MOI and/or LOI values, and as can be seen from Table 1 the reported LOI value was slightly higher for

sample A. The higher LOI value indicates more structural hydroxyls (OH groups retained after the calcination in the Bayer process) and thus a greater HF formation potential. What may also be seen is a sharp weight loss at around 270°C for both aluminas; this indicates the presence of residual gibbsite (or un-calcined material) in the alumina. When heated, gibbsite starts to transform to boehmite and/or transition alumina at around 250°C (depending on the reaction conditions). In the thermogram below (**figure 1**, blue line) this can be seen as a rapid loss of mass (starting at around 250°C) as the OH-groups in the gibbsite reacts to form H_2O. The residual gibbsite in the alumina has the potential to react with the electrolyte to form HF, but is obviously not accounted for by the LOI (300-1000°C) value. The MOI (50-300°C) value is typically associated with, and dominated by, the surface water/moisture, although, when gibbsite is present it will be included in the MOI value.

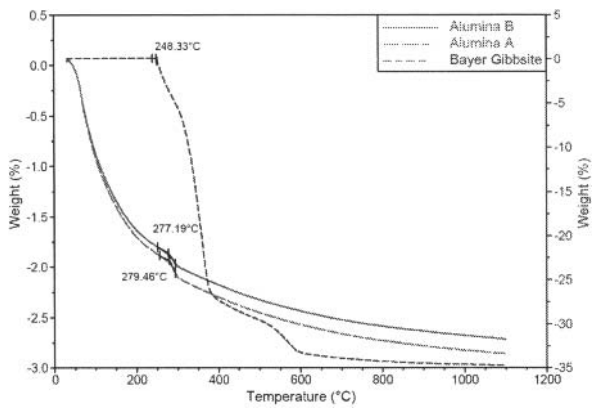

Figure 1. Thermograms for the two of the alumina samples: alumina A (red dashed line, left y-axis) and alumina B (green line, left y-axis) as well as a reference gibbsite sample (blue solid line, right y-axis).

Thus, in order to account for the gibbsite as a potential source for HF formation, the temperature limits for the MOI and LOI values need to be re-evaluated. When gibbsite is present in the alumina a more appropriate measurement of the surface water/moisture (less likely to be transported into the electrolyte and react to form HF) is perhaps the weight loss between 50 and 250°C. An LOI value from 250 to 1100°C would then account for both the residual OH and the gibbsite, the primary HF sources. The 'new' limits can be seen in **Figure 2**. Note, however that although this is perhaps a more useful way to specify the MOI/LOI limits when gibbsite is present, the 'exact' limits for when surface water and/or residual OH is removed cannot be specified as these overlap to some extent. Also, as will be discussed later, not all H_2O released from the gibbsite is likely to react with the bath to form HF (the gibbsite dehydroxlation reaction at high temperatures is very rapid and some water will flash off without coming in contact with the bath).

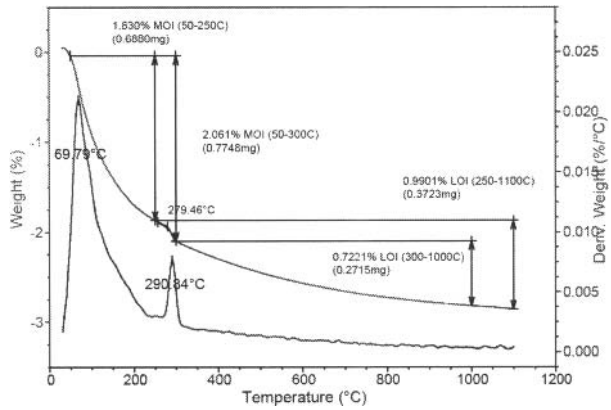

Figure 2. Thermogram for alumina A with the MOI and LOI limits indicated. The blue line is the derivative weight loss (wt-% $°C^{-1}$) which is a way to better identify specific phase transitions.

To estimate the HF generation potential of alumina, the LOI value provides a reasonable estimate of the amount of reactive OH, particularly when the extended range (250-1100°C) is considered. However, when gibbsite and/or boehmite are present in the alumina these components should also be quantified and reported. For this a number of methods have been suggested, such as: DSC [18] Near Infrared Spectroscopy [19] and quantitative XRD, employed in this study and elsewhere [15, 20]. Although readily available, these methods have not been widely adopted in the industry for routine characterisation. Table 3 provides this comparative data for the samples considered in this study.

Table 3. Additional characterisation data for the four aluminas: MOI (to 300°C) and LOI (300-1000°C and 250-1100°C) values (by TGA), surface area, average pore size and total pore volume (by nitrogen porosimetry), and gibbsite and alpha alumina content (by XRD with Rietveld refinement).

	Alumina A	Alumina B	Alumina C	Alumina D
MOI (to 300°C) wt-%	2.061	1.954	2.478	2.645
LOI (300-1000°C) wt-%	0.722	0.682	1.014	1.052
LOI (250-1100°C) wt-%	0.990	0.917	1.523	1.448
BET-Surface Area m2g-1	68.1	69.0	70.7	76.1
BJH-Pore Size nm	5.78	5.70	8.78	11.20
BJH-Pore Volume cm3g-1	0.210	0.215	0.193	0.207
Gibbsite wt-%	0.93	0.56	1.98	2.65
Alpha wt-%	8.1	7.6	3.9	6.5

The inevitable effect of residual gibbsite is that a large amount of water (as OH) enters the cell with the alumina. As can be seen from the thermogram in **figure 1**, approximately 35 wt-% of gibbsite will react to form H_2O when heated. This will occur very rapidly when it comes in contact with the electrolyte, inducing a phase transition into the transition aluminas. The phase transition, will be competitive with dissolution but the very rapid formation of large amounts of water vapour will create a volcano effect, carrying fine particles out of the cell and potentially increasing dusting.

Assuming that all OH in the gibbsite reacts to form H_2O and Al_2O_3 (according to reaction 1),

$$2Al(OH)_3(s) + E_1 \rightarrow Al_2O_3(s) + 3H_2O(g) \qquad /1/$$

where E_1 is the reaction energy, a theoretical increase in the energy demand can be calculated. Based on the amount of water that is evolved the additional (apart from the structural hydroxyl, measured by the LOI tests) HF generated due to the gibbsite in the SGA can also be calculated. To calculate the increased HF generation capacity due to gibbsite in the alumina it is assumed that all H_2O will react according to reaction 2:

$$3H_2O(g) + 2AlF_3(g/s) \rightarrow 6HF(g) + Al_2O_3(diss) \qquad /2/$$

In practice it is not likely that all H_2O will react to form HF (as some will obviously exit the cell with the off gases). It should be noted that the HF lost to the environment (due to the incomplete capture) constitutes a direct loss of bath, which will have to be supplemented. Depending on the gibbsite content this may have a significant economic impact if particulate and gaseous emissions are not fully captured.

XRD analyses revealed that 0.93 and 0.56 wt-% of alumina A and B, respectively, is gibbsite. Assuming that 1.92 kg of alumina is needed to produce 1 kg of aluminium metal it is then calculated that 18 and 11kg of gibbsite is introduced, for alumina A and B, respectively, to the cell per metric ton of Al produced. Based on the reactions above we can then also calculate that the 0.93 and 0.56 wt-% of gibbsite in the aluminas results in an additional 8.2 and 5.0 kg of HF being formed per ton of Al metal, for alumina A and B, respectively, on top of the 'background' HF from the structural hydroxyls (reflected in the LOI value). The additional HF due to the presence of (0.93 wt-%) gibbsite is about 20% of the total (theoretical) HF. Although these are theoretical maximum HF levels (based on complete reactions) it can be seen that even small amounts of gibbsite in the alumina have the potential to significantly increase the total HF burden.

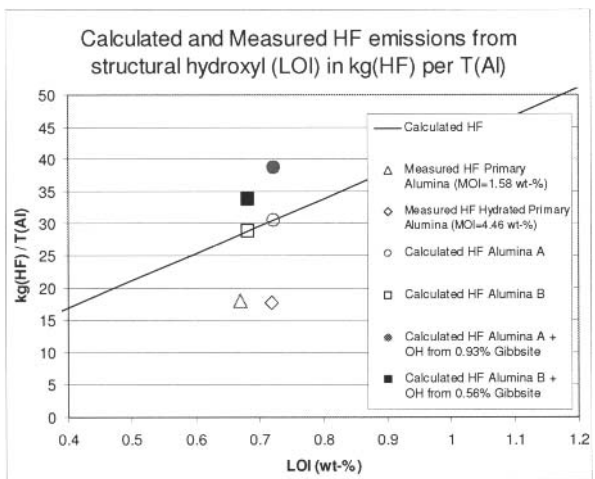

Figure 3. Theoretical HF generation capacity (calculated based on equations 1 and 2) and measured HF generated by structural hydroxyls in the alumina (numerical values sourced from ref. [7]).

In figure 3 calculated (solid line), based on reaction 2, HF generation *capacities* are plotted as a function of their LOI values. For comparison two measured HF emission values for aluminas with known MOI and LOI values are included. Not surprisingly the measured values are slightly lower than the calculated ones, but should still provide a reasonable estimate of the HF generation capacity. The measured values were sourced from the literature [7]. In the study dry and 'hydrated' alumina samples were fed to a plant cell and the resulting HF emissions measured. It can be seen that the MOI, or moisture content, has little or no contribution to the HF emissions.

Figure 4 displays HF measurements (GTC inlet and outlet levels) when aluminas C and D were used. The higher inlet GTC HF concentration when alumina D was used may be attributed to the slightly higher gibbsite content. However, the gibbsite content alone could not explain the significantly poorer performance of alumina D in terms of HF removal. To understand the performance of these aluminas the porosity and microstructure needs to be evaluated as well. A direct relationship between specific surface area and HF adsorption capacity has been reported [3]. High specific surface area is often considered advantageous in terms of optimal dry scrubber performance, and can often be the only way to deal with increased fluoride emissions. There is also a relationship between surface area and residual hydroxyl content. The residual hydroxyls are retained in the crystal lattice of the transition alumina phases due to incomplete calcination of gibbsite. In other words, higher surface area stems from more of the low order transition aluminas (gamma, chi, rho alumina) which also have more residual hydroxyls retained in the lattice and hence also have a higher HF generation potential.

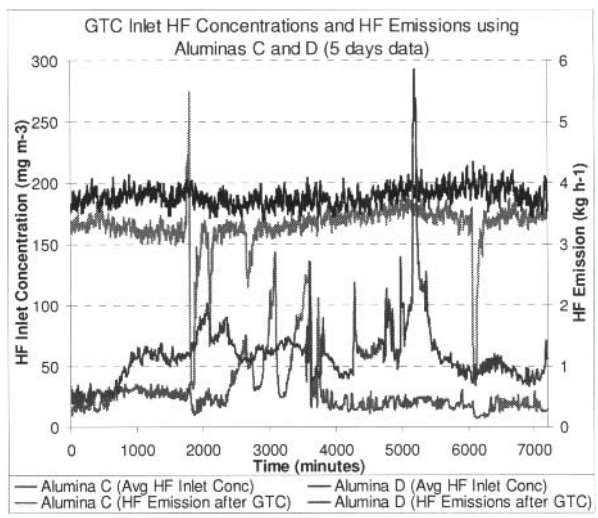

Figure 4. Dry scrubber (GTC) inlet HF concentrations and corresponding HF emissions when using aluminas C and D (5 days data).

The pore size distribution and mean pore size, as well as surface area are a measure of the extent of the calcination reactions [5]. As the calcination reactions progress, the pore size grows, but pores coalesce, causing the surface area to decrease as a result. A narrow pore size distribution in a range that allows HF molecules to be easily transported to internal surfaces and reactive sites is desired and results from a well controlled calcination process. Pore size distribution is also an effective way to identify if the

alumina is blended. A mixture of two differently calcined aluminas, or an alumina containing under- or over calcined material will result in a broad pore size distribution or a distinctly bimodal distribution. For a well-controlled calcination process, a narrow pore size distribution centred around 6-8 nm is typically observed, and desired (see figure 5). Higher calcination temperatures or longer calcination times usually result in an increased pore size and highly over-calcined material (more theta-alpha alumina) shows up as a peak at >10 nm pore sizes. Material with a lower degree of calcination results in a lower average pore size and generally shows as a peak in the <2 nm pore size range on the distribution plots. Poor control of the calcination process results in a broader peak in the 4-10 nm pore size range.

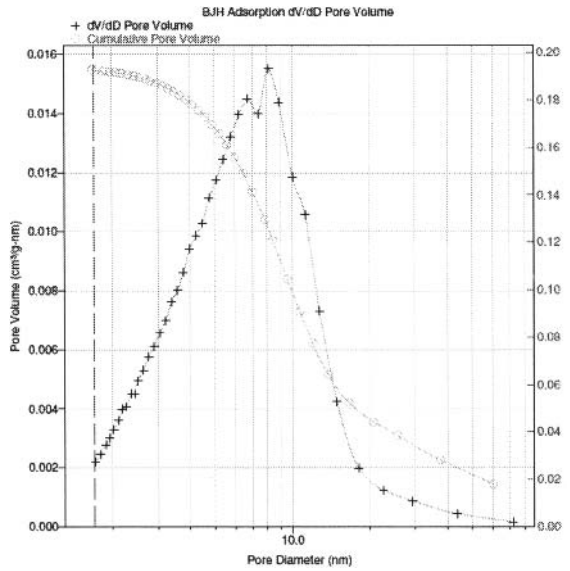

Figure 5. BJH pore size evaluations for alumina C reveals a 'normal' pore size distribution.

As reported in table 3, the surface area measurements revealed that alumina D had a slightly higher surface area than alumina C (76.1 and 70.7 m^2/g, respectively) which could be assumed to improve the dry-scrubbing efficiency and offset some of the additional HF that is likely to be generated by the higher LOI content. However, when the pore size distribution plots are examined (figures 5 and 6) some interesting differences between the two samples can be seen. Alumina C shows one peak at a pore size of approximately 8 nm whereas alumina D clearly has a bimodal pore size distribution with one peak centred below the 1.0 nm pore size limit of this technique, and the other centred at a much larger pore size of approximately 12 nm. This would indicate that alumina D contains a large quantity of under-calcined material and that the rest of the sample is over-calcined (rich in theta and alpha alumina). As the small pores contribute more to the total (or average) surface area the alumina D therefore has a larger nitrogen specific surface area. Note that by controlling the calcination conditions, surface areas in excess of 350 m^2g^{-1} may be achieved.

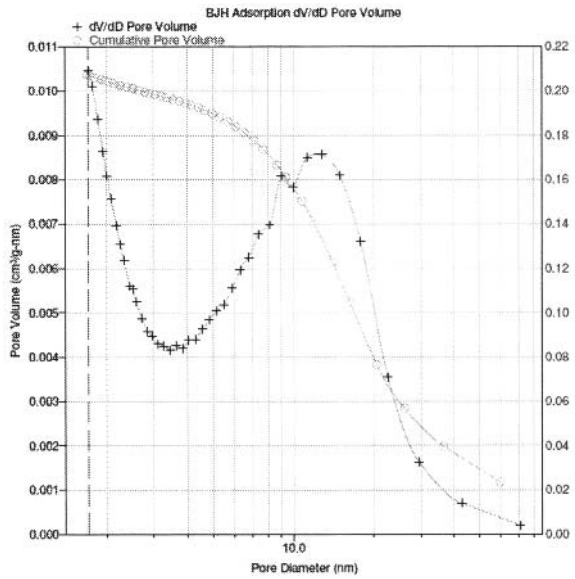

Figure 6. More than one way to achieve a surface area target. Alumina D displayed a distinctly bi-modal pore size distribution, indicating the presence of under-calcined components as well as over calcined material.

From an operational viewpoint the blend of over- and under calcined material is detrimental for a number of reasons. As mentioned previously the low order transition aluminas contain more residual hydroxyls (confirmed by the LOI measurements) resulting in more HF generation upon dissolution. At the same time, the fine pore size is likely detrimental for HF removal. The narrow pores restrict access to internal porosity and readily become blocked (when HF reacts to form oxy-fluorides). This further restricts access to internal sites, thus reducing the capacity and rate of HF absorption. Moreover, the over-calcined components in the sample are likely to have a poor dissolution rate. Thus, the currently used surface area specification, derived under equilibrium conditions is not ideal for predicting scrubbing efficiency and it would be helpful to extended this to include information about the pore size distribution. This information is readily available using most of the commercial surface area instruments by examining the nitrogen adsorption isotherms using the BJH method.

Conclusions

Plant measurements and additional laboratory characterization of a number of alumina samples was used to highlight some of the shortcomings of the alumina specifications sheet when it comes to understanding alumina performance, particularly with regards to HF generation and emissions as well as feeding and dissolution characteristics. It was demonstrated that residual gibbsite in the alumina results in increased HF levels (which coupled with poor hooding/collection efficiency results in an additional loss of electrolyte) and feeding perturbations. Therefore, knowing the amount of gibbsite in the alumina will help to predict and control the process response to the alumina quality. Several low cost options for determining the gibbsite content in alumina exist (XRD, NIR, DSC or TGA for example) and should be adopted more widely.

Nitrogen porosimetry and investigations of alumina microstructure revealed that the low order transition aluminas (gamma, chi, rho alumina) have a limited pore size and plant measurements indicate that this is detrimental for the dry-scrubbing process. It seems that the narrow pores, although resulting in large average surface areas, may become blocked thus restricting access to internal surfaces which effects the HF adsorption capacity adversely (at the same conditions). These observations indicate that a pore size distribution specification would be a better requirement for alumina quality (than a single surface area target) as this ensures good scrubbing and may even be energetically favorable in the alumina refinery. The pore size distribution may readily be measured through nitrogen adsorption techniques using existing equipment both in the smelters and alumina refineries.

Acknowledgements

The authors would like to thank Anita Folkers and Karin Bouwmeester for their assistance with the alumina samples and HF measurements, the interpretation of the results and their contributions to this manuscript.

References

1. Wellwood, G.A., *The practice of dry scrubbing.* Light Metals (Warrendale, PA, United States), 2001: p. 371-377.
2. Zhang, W., X. Liu, P. McMaster, and M. Taylor, *Modeling of impurity balance for an aluminum smelter.* Light Metals (Warrendale, PA, United States), 1996: p. 405-11.
3. Gillespie, A.R., *Mechanistic Studies of HF Adsorption on Alumina.* PhD Thesis, The University of Auckland, New Zealand, 1997.
4. Gillespie, A.R., M.M. Hyland, and J.B. Metson, *Irreversible HF adsorption in the dry-scrubbing process.* Journal of Metals, 1999. **51**(5): p. 30-32.
5. Perander, L., *Evolution of Nano- and Microstructure During the Calcination of Bayer Gibbsite.* PhD Thesis, The University of Auckland, New Zealand, 2010.
6. Patterson, E.C., *Hydrogen Fluoride Emissions From Aluminium Electrolysis Cells.* PhD Thesis, The University of Auckland, New Zealand, 2002.
7. Hyland, M., E. Patterson, and B. Welch, *Alumina structural hydroxyl as a continuous source of HF.* Light Metals (Warrendale, PA, United States), 2004: p. 361-366.
8. Haverkamp, R.G., *Surface studies and dissolution studies of fluorinated alumina.* PhD Thesis, The University of Auckland, New Zealand, 1992.
9. *Aluminium oxide primarily used for the production of aluminium - Determination of loss of mass at 300°C and 1000°C.* ISO 806:2004.
10. Brunauer, S., P.H. Emmett, and E. Teller, *Adsorption of gases in multimolecular layers.* Journal of the American Chemical Society, 1938. **60**: p. 309-19.
11. Barrett, E.P., L.G. Joyner, and P.P. Halenda, *The determination of pore volume and area distributions in porous substances. I. Computations from nitrogen isotherms.* Journal of the American Chemical Society, 1951. **73**: p. 373-80.
12. Rietveld, H.M., *Line profiles of neutron powder-diffraction peaks for structure refinement.* Acta Crystallographica, 1967. **22**(1): p. 151-2.
13. Rietveld, H.M., *Profile refinement method for nuclear and magnetic structures.* Journal of Applied Crystallography, 1969. **2**(Pt. 2): p. 65-71.
14. Rodriguez-Carvajal, J. *FULLPROF: A Program for Rietveld Refinement and Pattern Matching Analysis.* in *Abstracts of the Satellite Meeting on Powder Diffraction of the XV Congress of the IUCr.* 1990. Toulouse, France.
15. Perander, L.M., Z.D. Zujovic, T. Groutso, M.M. Hyland, M.E. Smith, L.A. O'Dell, and J.B. Metson, *Characterization of metallurgical-grade aluminas and their precursors by 27Al NMR and XRD.* Canadian Journal of Chemistry, 2007. **85**(10): p. 889-897.
16. Perander, L.M., Z.D. Zujovic, M.M. Hyland, M.E. Smith, L.A. O'Dell, and J.B. Metson, *Short- and long-range order in smelter grade alumina - Development of nano- and microstructures during the calcination of Bayer Gibbsite.* Light Metals (Warrendale, PA, United States), 2008: p. 29-35.
17. Perander, L.M., Z.D. Zujovic, T.F. Kemp, M.E. Smith, and J.B. Metson, *The Nature and Impacts of Fines in SGA.* Journal of Metals, 2009. **61**(11): p. 33-39.
18. Wehrli, J.T. and A.R. Kane, *Application of differential scanning calorimetry for characterization of Bayer process solids.* Light Metals (Warrendale, PA, United States), 1993: p. 175-84.
19. Dando, K.R. and N.R. Dando, *Rapid, non-destructive analysis of % gibbsite in smelting grade alumina.* Light Metals (Warrendale, PA, United States), 2010: p. 531-533.
20. Whittington, B. and D. Ilievski, *Determination of the gibbsite dehydration reaction pathway at conditions relevant to Bayer refineries.* Chemical Engineering Journal (Amsterdam, Netherlands), 2004. **98**(1-2): p. 89-97.